

Article

Numerical Investigation on Suction Flow Control Technology for a Blunt Trailing Edge Hydrofoil

Peng Yang^{1,2,3}, Chiye Zhang⁴, Hongyeyu Yan^{1,2}, Yifan Ren¹, Changliang Ye^{1,3,*} , Yaguang Heng⁵ 
and Yuan Zheng^{1,3}

¹ College of Energy and Electrical Engineering, Hohai University, Nanjing 211100, China; 2020020214@hhu.edu.cn (P.Y.); 2020020215@hhu.edu.cn (H.Y.); 2105060119@hhu.edu.cn (Y.R.); zhengyuan@hhu.edu.cn (Y.Z.)

² Hohai-Lille College, Hohai University, Nanjing 211100, China

³ College of Water Conservancy and Hydropower, Hohai University, Nanjing 210098, China

⁴ China Institute of Water Resources and Hydropower Research, Beijing 100038, China; chiye0214@hotmail.com

⁵ Key Laboratory of Fluid and Power Machinery of Ministry of Education, Xihua University, Chengdu 610039, China; hengyaguang@gmail.com

* Correspondence: yechangliang@hhu.edu.cn

Abstract: The generation of hydro-mechanical resonance is related to the transition of the boundary layer and the development of vortex shedding. The application effect of suction control in hydrodynamics is equally deserving of consideration as an active control technique in aerodynamics. This study examines how suction control affects the flow field of the NACA0009 blunt trailing edge hydrofoil using the γ transition model. Firstly, the accuracy of the numerical method is checked by performing a three-dimensional hydrofoil numerical simulation. Based on this, three-dimensional hydrofoil suction control research is conducted. According to the results, the suction control increases the velocity gradient in the boundary layer and delays the position of transition. The frequency of vortex shedding in the wake region lowers, and the peak value of velocity fluctuation declines. The hydrofoil hydrodynamic performance may be successfully improved with a proper selection of the suction coefficient via research of the suction coefficient and suction position on the flow field around the hydrofoil. The lift/drag ratio goes up as the suction coefficient goes up. The boundary layer displacement thickness and momentum thickness are at their lowest points, and the velocity fluctuation amplitude in the wake region is at its lowest point as the suction coefficient $C_\mu = 0.003$. When the suction slots are at the leading edge, the momentum loss in the boundary layer is minimal and the velocity fluctuation in the wake zone is negligible.

Keywords: blunt trailing edge hydrofoil; suction control; boundary layer; transition model

MSC: 76-10



Citation: Yang, P.; Zhang, C.; Yan, H.; Ren, Y.; Ye, C.; Heng, Y.; Zheng, Y. Numerical Investigation on Suction Flow Control Technology for a Blunt Trailing Edge Hydrofoil. *Mathematics* **2023**, *11*, 3618. <https://doi.org/10.3390/math11163618>

Academic Editor: Marco Pedroni

Received: 31 July 2023

Revised: 17 August 2023

Accepted: 18 August 2023

Published: 21 August 2023



Copyright: © 2023 by the authors. Licensee MDPI, Basel, Switzerland. This article is an open access article distributed under the terms and conditions of the Creative Commons Attribution (CC BY) license (<https://creativecommons.org/licenses/by/4.0/>).

1. Introduction

One of the main causes of the pressure pulsation of hydraulic machinery is the vortex shedding in the wake area, and the pressure pulsation will affect the operation stability of hydraulic units [1]. The primary goal of hydraulic machinery research has always been the regulation of the flow field [2]. At present, the commonly used flow control includes active control and passive control. Injecting energy into the flow field is not required for passive control, and the control mode cannot vary with the change in flow state, such as vortex generator, tail modification and wingtip device. Active flow control requires external energy injection, that is, the control scheme can be adjusted according to the specific flow field conditions during the operation of the turbomachinery to change the flow field structure, such as plasma, artificial jets, and boundary layer blowing and suction. Active control can control complex dynamic systems accordingly and has been widely used in recent years [3–5].

Prandtl [6] successfully controlled the boundary layer separation flow by using boundary layer suction technology to the cylinder flow field. Later, suction technology was further studied in aerodynamic research. The results of these studies show that suction and blowing significantly affect lift and drag coefficients by shifting the pattern of pressure across the airfoil's surface [7,8]. In addition, the methods of air blowing, suction, and synthetic jet have been used to study NACA airfoils [9,10]. Chen [11] researched the suction and blowing flow field control technology of the NACA0012 airfoil and discovered that when the nozzle position and angle of attack are combined, the lift coefficient can be improved by the vertical intake suction at the leading edge more than other suction conditions, and the lift coefficient can be increased by the tangential inlet blowing at the trailing edge. Rosas [12] applied the numerical simulation method to inject oscillatory fluid into the flow field, and the results showed that this method can dramatically increase the airfoil's lift coefficient. Beliganur [13] controlled the flow field using the optimization algorithm, which showed that the NACA0012 airfoil lift/drag ratio was improved by using two suction nozzles and two blowing nozzles. Akcayoz [14] investigated how to enhance the function of the NACA0015 airfoil by optimizing the synthetic injection parameters at diverse angles of attack, using the highest lift/drag ratio as the optimization goal, and concluded that the ideal injection position is at the leading edge of the airfoil. When the angle of attack increases, the best injection angle also increases. Muddada [15] looked into the impact of porous suction on the separated flow at the low Reynolds number on the surface of the airfoil. According to the study, as the suction coefficient rose, the lift/drag ratio first rose quickly and then declined gradually. The influence of the suction area was also analyzed in detail, and it was found that the suction area with the largest lift/drag ratio is located behind the separation point. The influence of slot spacing and slot diameter is small. Ramsay [16] simulated a three-dimensional cylinder with three suction slots and concluded that the aerodynamic performance could be the best when the suction angle is 90° or 270° and the suction position is near the separation point. In the study of flow control of hydraulic machinery, Akbarzadeh [17] and De Giorgi [18] reached the conclusion that the pore structure can improve the cavitation phenomenon. Royset [19] evaluated how the marine hydrofoil lift and drag coefficients changed with the suction method and found that the lift coefficient was improved in the process of water spray and micro-absorption. To investigate the impact of various suction factors on the hydrofoil, Wang [20] chose a two-dimensional symmetric hydrofoil. In the study, he found suction control can enhance hydrodynamic performance. As the distance between the suction ports is uplifted, the lift coefficient falls. As the suction ports move to the back edge, the hydrofoil's lift/drag ratio rises, and as the suction ports become wider, the lift/drag ratio changes. Goodarzi [21] adopted the two-dimensional NACA0015 hydrofoil; analyzed the hydrodynamic performance of the hydrofoil with a nozzle; discussed the influence of the nozzle position, injection speed, injection angle and other parameters on the hydrodynamic performance; and proved that the installation of the nozzle can enhance performance on a broad frontal angle and postpone the boundary layer's separation. Chen [22] examined the effects of leading-edge suction on the hydrodynamic performance of a hydrofoil and discovered that increasing the suction inlet at the leading edge can reduce the stall angle, increase the range of stable working angle, increase the drag coefficient, and enhance the hydrofoil performance. Yousefi [23] analyzed the hydrodynamic performance of the installed nozzle, the nozzle with the suction method, and the injection combined hydrofoil, and found that when the nozzle direction is tangential, the nozzle width is 3.5–4% of the chord length, and the lift/drag ratio is the largest. On the contrary, if the nozzle is vertical, the lift/drag ratio decreases linearly, and the optimal width value decreases; the lift/drag ratio rises as the suction opening width grows, peaking at 2.5% chord length, when the suction opening width is at its widest.

The early flow control research is mainly based on experiments [24,25]. Because of the advancement of CFD technologies, more and more scholars study suction control via numerical simulation. The hydrofoil boundary layer's transitional properties are impacted

by flow control, which then has an impact on the hydrofoil's flow properties, for instance, lift and drag, flow separation, and wake shedding. Therefore, accurately predicting the transition phenomenon is very necessary. At present, the numerical methods that have been successfully applied to the boundary layer flow transition include the e^N method, the transition empirical formula method, and the low Reynolds number model method [26]. In the engineering field, the impact of transition is frequently considered via numerical simulation, and the most widely used is the Gamma-Theta proposed by Langtry and Menter ($\gamma-Re_{\theta t}$) transition model [27], which relies entirely on local variables and can be coupled with other turbulence models without much modification. In the coupling of all turbulence models, the SST $\gamma-Re_{\theta t}$, in addition to the SST $k-\omega$ turbulence model, is the most widely utilized, not just for aerodynamics transition and separation prediction [28] but also in the field of hydraulics. Rahman [29], Zeng [30,31], and Ye [32,33] used the SST $\gamma-Re_{\theta t}$ to the boundary laminar flow of hydrofoil, which transits along the middle and low Reynolds numbers, and the transition of hydrofoil hydrodynamics is analyzed. However, the model needs to solve the batch factor equation and the transition criterion equation at the same time, and the calculation is slightly cumbersome. In 2015, Menter [34] simplified the $\gamma-Re_{\theta t}$ transition model to the gamma (γ) transition model that uses the notion of local variables, which can predict various transition processes and meet Galilean invariant. Wang [35], Cui [36], and Rubino [37] use different test examples to verify the model and obtain better prediction results.

According to the research, the studies mentioned have contributed valuable insights to flow control and hydrodynamic performance improvement. However, there are some notable shortcomings that can be improved. First, limited real-world validation: Many of these studies rely heavily on numerical simulations and simplified models. More real-world validation via experiments under various conditions is needed to ensure the applicability and accuracy of the findings. Second, insufficient understanding of complex flows: Some of the studies may oversimplify the flow conditions or not fully consider the complexities of turbulent or unsteady flows. A deeper understanding of the underlying flow physics is necessary for effective control strategies. Finally, the numerical simulation of suction control is mainly focused on aerospace dynamics. Most of the research objects are airfoils with medium and low Reynolds numbers. In this research, the three-dimensional NACA0009 blunt trailing edge hydrofoil with an angle of attack of 0° at a high Reynolds number ($Re_L = 2.0 \times 10^6$) is numerically simulated to reveal the unsteady properties of the flow field. Suction slots are then placed on the hydrofoil's upper surface to manage the flow field. Finally, the influence of suction parameters on the boundary layer flow, vortex shedding frequency and velocity distribution near the wake area are explored.

2. Model and Numerical Techniques

2.1. Geometry

The NACA0009 [38] blunt trailing hydrofoil is chosen for research, which was tested at Swiss Federal Institute of Technology in Lausanne, Switzerland. The chord length L is 0.1 m, with spanwise width $B = 0.15$ m; in addition, the thickness of the trailing edge is equal to 3.22×10^{-3} m, and 0° of angle of attack is selected for research. The geometric configuration is presented in Figure 1.

The inlet boundary is $3L$ from the hydrofoil leading edge, the outlet boundary is $5L$ from the trailing edge, and the upper and lower boundaries are $0.75L$ from the leading edge. Figure 2 displays the computation domain. The reason for selecting a Z-axis length of $0.3L$ in the 3D computational domain was a careful consideration aimed at achieving a balance between computational efficiency and capturing the essential flow characteristics.

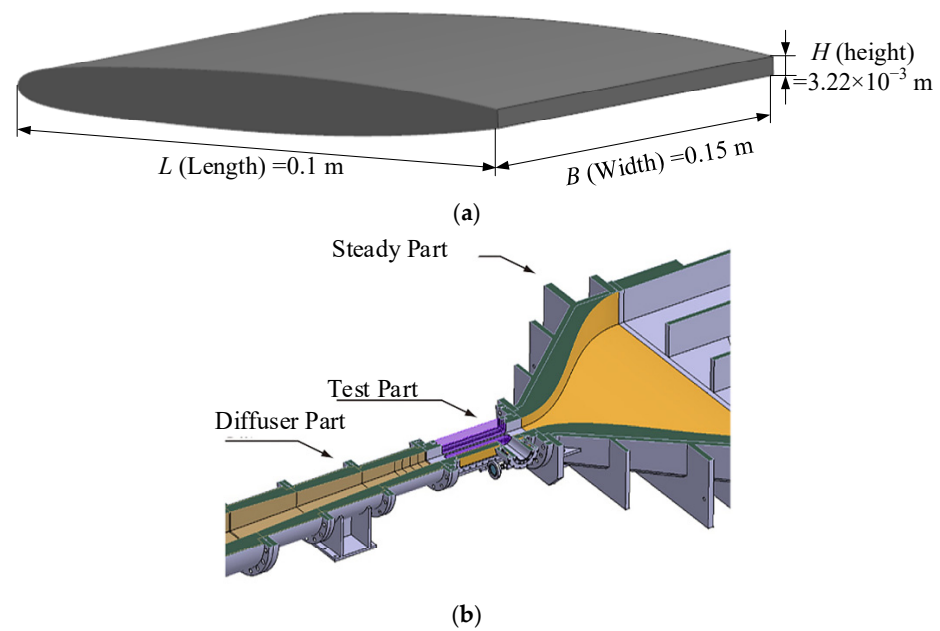


Figure 1. NACA0009 blunt trailing-edge hydrofoil. (a) hydrofoil; (b) test rig [38] (Ausoni, 2009).

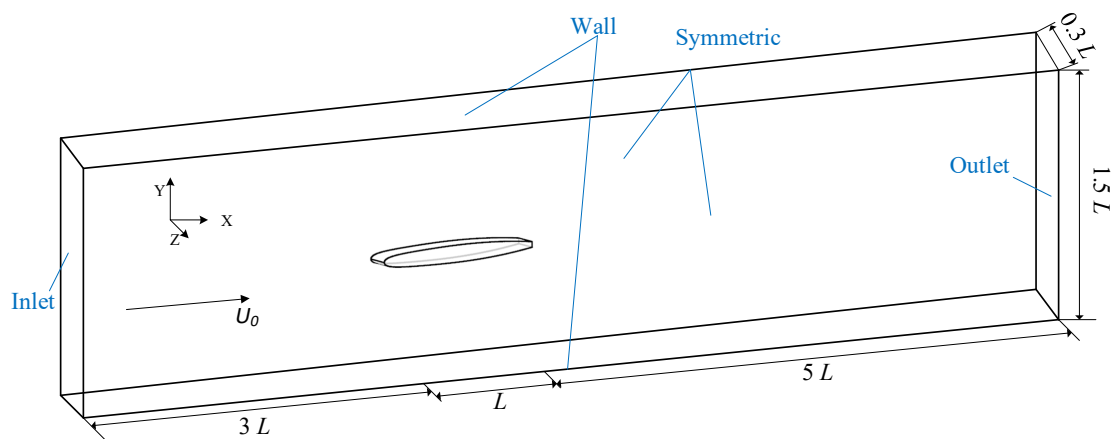


Figure 2. 3D computation domain.

2.2. Turbulence Models

Menter and Smirnov proposed the γ transition model [34], which is on the basis of the $\gamma-Re_{\theta_t}$ transition model. The transition critical momentum thickness Reynolds number Re_{θ_c} in this model can be directly solved by variables in the boundary layer, thus replacing the Re_{θ_t} transport equation. The expression of the γ transport equation is:

$$\frac{\partial \rho \gamma}{\partial t} + \frac{\partial (\rho u_j \gamma)}{\partial x_j} = P_\gamma - E_\gamma + \frac{\partial}{\partial x_j} \left(\left(\mu + \frac{\mu_t}{\sigma_\gamma} \right) \frac{\partial \gamma}{\partial x_j} \right) \tag{1}$$

The generation term and destruction term in the source term work together to control the size of the intermittent factor. The definition formula of P_γ and E_γ are as follows:

$$P_\gamma = F_{\text{length}} \rho S \gamma (1 - \gamma) F_{\text{onset}}, \quad E_\gamma = c_{a2} \rho \Omega \gamma F_{\text{turb}} (c_{e2} \gamma - 1) \tag{2}$$

In the formula, F_{length} is the amount of transition zone length, which is used to control the size of the generation term; F_{onset} is the function that triggers the growth of the intermittent factor; c_{a2} and c_{e2} are constant coefficients; Ω is the vorticity; and F_{turb} is

applied to eliminate the destruction term’s influence on the flow outside of the laminar boundary layer or the viscous bottom layer, and its expression is as follows:

$$F_{\text{turb}} = e^{-\left(\frac{R_T}{2}\right)^4} \tag{3}$$

The expression of Re_{θ_c} is as follows:

$$Re_{\theta_c}(Tu_L, \lambda_{\theta L}) = C_{Tu1} + C_{Tu2} \exp[-C_{Tu3} Tu_L F_{PG}(\lambda_{\theta L})] \tag{4}$$

In the above formula, constant coefficients C_{Tu1} and C_{Tu2} control Re_{θ_c} . From the correlation formula, the minimum value of Re_{θ_c} is C_{Tu1} at high turbulence intensity level, and the maximum value at a low turbulence intensity level is the sum of C_{Tu1} and C_{Tu2} . Constant coefficient C_{Tu3} controls Re_{θ_c} decreases with the increase in turbulence intensity Tu_L . $F_{PG}(\lambda_{\theta L})$ is dependent on the parameter for the pressure gradient λ_{θ} , which serves to illustrate the reflection of the pressure gradient parameter $\lambda_{\theta L}$ on the Reynolds number of the transition critical momentum thickness.

The turbulent kinetic energy transfer equation’s source term is corrected to couple the γ transition model with the SST $k-\omega$ turbulence model. The transport equation of the coupled turbulent kinetic energy k is given below:

$$\frac{\partial}{\partial t}(\rho k) + \frac{\partial}{\partial x_j}(\rho u_j k) = \bar{P}_k + P_k^{lim} - \bar{D}_k + \frac{\partial}{\partial x_j} \left[(\mu + \sigma_k \mu_t) \frac{\partial k}{\partial x_j} \right] \tag{5}$$

$$\bar{P}_k = \gamma P_k, \bar{D}_k = \max(\gamma, 0.1) \cdot D_k, P_k = \mu_t S \Omega \tag{6}$$

In the source term, to avoid overestimating the turbulence intensity in the stagnation zone, the P_k and D_k terms in the SST $k-\omega$ model were revised. The term accelerates the boundary layer creation of turbulent kinetic energy when the turbulence intensity is low. As soon as the boundary layer transition procedure is finished, the term will lose its function. Specific parameters of the γ transition model could be found in the literature [34].

2.3. Numerical Method and Mesh

This section first gives the unsteady flow boundary conditions of hydrofoil without suction measures, and the suction boundary conditions will be described in the following chapters. The boundary setting is shown in Table 1. The inlet boundary has a specified inlet velocity. The outlet boundary is specified by the pressure outlet, and the given relative pressure value is 0 Pa. The hydrofoil surface is a non-slip wall (three components of wall velocity, respectively). Symmetric boundary conditions are given for the front and rear boundaries (z direction) of the computational domain. To solve the above equations, it is necessary to discretize the entire computational domain of the hydrofoil, that is, divide the continuous computational domain in space into multiple sub-regions, then determine the nodes in each sub-region, and finally generate a grid. The finite volume method has the characteristics of high computational efficiency. For the simulation of hydrofoil, in order to discretize the control equation, the finite volume method is employed. The transient problem has more transient terms related to time than the steady-state problem. The fully implicit scheme has low requirements for the time step, that is, its solution will not oscillate due to the selection of the time step, which is unconditionally stable. This scheme has been widely used in the process of solving transient problems [39]. Based on the advantages of the implicit time scheme, it is chosen to discretize the temporal domain in this computational experiment. For both the diffusion and the source terms, the upwind difference of the second order is used in the convection term. whereas the central difference with second-order precision is applied for interpolation on the interface. This study was completed on the ANSYS CFX 2022 platform. 256 GB of memory and 128 parallel processing cores were used to run this portion of the calculation in Hohai University’s high-performance computing facility.

Table 1. Boundary setting.

Input Parameter	Magnitude	Input Parameter	Magnitude
Time analysis	Unsteady	Temperature	25 °C
Density of fluid	Water (998.2 kg/m ³)	Wall	No slip
Reynolds number	Vary with inlet velocity	Length	0.1 m
Angle of attack	0°	Dynamic viscosity	0.001003 kg/(m·s)

The hydrofoil grid is divided using ICEM CFD, and the computational domain is discretized using a hexagonal structural grid. Considering the geometric characteristics of the trailing edge, the mesh of the boundary layer is densified, and the O-grid is used for the hydrofoil. In accordance with the grid convergence index (GCI) extrapolation technique developed by Richardson [40], three sets of mesh are used for grid convergence analysis. The specific number of grids is shown in Table 2.

Table 2. Grid parameters.

Parameter	Value
N_1, N_2, N_3	3,615,753; 4,824,863; 6,275,698
r_{21}	1.33
r_{32}	1.27
P	11.02–13.18
P_{ave}	12.72
GCI	0.000006–0.367258%
GCI_{ave}	0.042535%

The local grid at the near wall and trailing edge of the hydrofoil are revised to increase computation precision and better reflect the fundamental properties. The grid scales in the x , y and z directions are $\Delta x = 1.01$ and $\Delta y = 0.53$, respectively. The initial layer of the grid that is located on the surface of the hydrofoil has a height of 0.0001 millimeter and the y^+ is 0.81. The total number of grid elements in the final selected calculation area is 6.2 million. Figure 3 shows the grid structure of the computing domain.

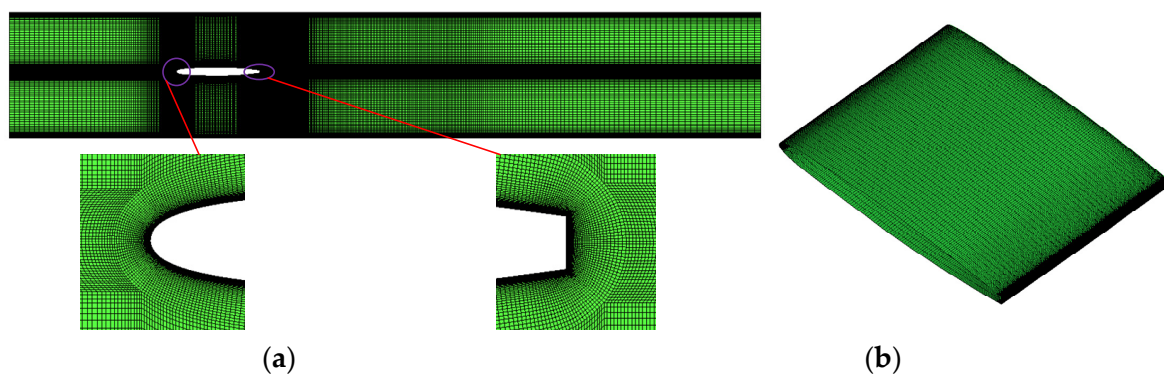


Figure 3. 3D computational domain grid. (a) Grid details on foil mid-plane; (b) spanwise GRID.

3. Verification

The three-dimensional hydrofoil in the reference state numerical simulation investigation revealed that there is an obvious three-dimensional feature in its span direction in the reference state. Therefore, in order to obtain accurate results, this chapter uses the three-dimensional hydrofoil for numerical calculation. The Reynolds number $Re_L = 2.0 \times 10^6$ is selected as the calculation condition in this section. The value of U_∞ , the entering flow velocity, is 20 m/s. To validate the methods used, the flow field structure of the hydrofoil is examined, and a portion of the calculation results are compared to the test data in this

section. Therefore, the numerical methods in this section are used as the basic state of flow control.

3.1. Friction Coefficient

The wall friction coefficient obtained using various models is displayed in Figure 4. Based on the findings, the SST $k-\omega$ model projected a greater wall friction coefficient than other models, indicating that the velocity gradient predicted by the SST $k-\omega$ model in this region is relatively low and the laminar boundary layer fails to be captured. The SST $\gamma-Re_{\theta_t}$ transition model and SST γ transition model are able to resolve the boundary layer transition flow, and the two models' anticipated transition completion positions are $0.83L$ and $0.86L$, respectively, indicating the SST $\gamma-Re_{\theta_t}$ premature prediction of the transition onset position.

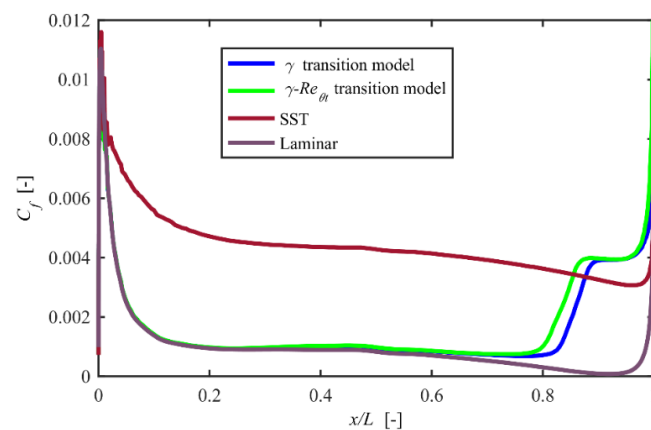


Figure 4. Distribution of hydrofoil surface friction coefficient along the flow direction.

3.2. Boundary Layer Thickness

The change in the hydrofoil boundary layer's relative thickness and form factor along the chord are depicted in Figures 5 and 6. The hydrofoil boundary layer thickness keeps growing from the leading edge, but at a relatively modest rate, but the growth rate becomes larger near the trailing edge. The numerical method's projected boundary layer thickness and the test value at the leading edge are both completely consistent, and at the trailing edge, it is thinner than the test value. However, the two have steadied varying tendencies.

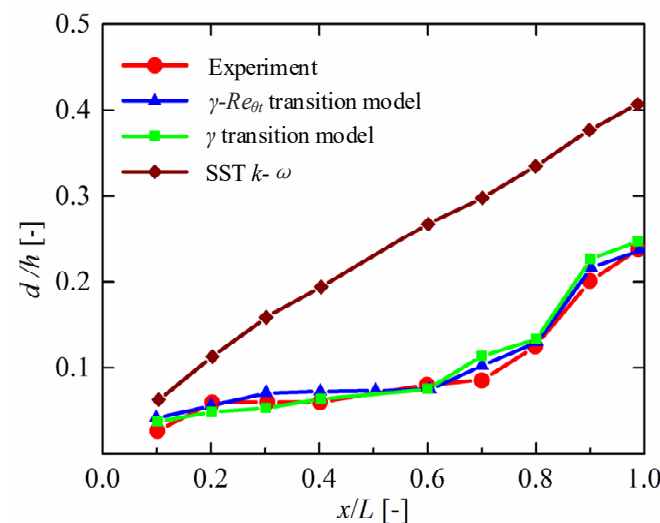


Figure 5. Relative thickness δ/h distribution of hydrofoil boundary layer at different models.

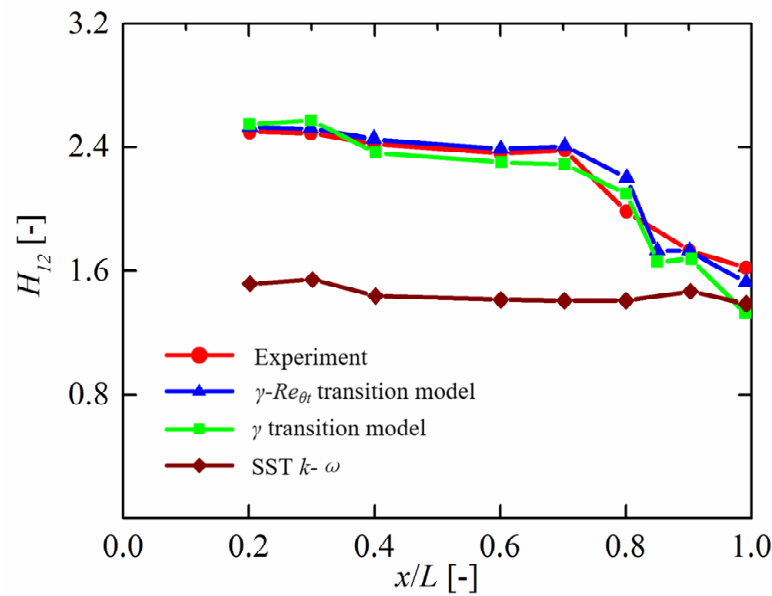


Figure 6. Distribution of hydrofoil boundary layer form factor H_{12} at different models.

3.3. Shedding Vortex Frequency

After the unsteady flow at the hydrofoil’s wake area monitoring point indicates periodic flow, the instantaneous velocity of the flow direction in four flow periods is chosen for a fast Fourier transform to analyze the frequency of the vortex shedding in order to determine the characteristics of the vortex in the wake area. Table 3 compares the test value and the numerical simulation vortex shedding frequency. From the table, the predicted frequency of the γ transition model is less than the measured value of the test, and the relative error of frequency is 2.1%, which demonstrates the reliability of the calculation method. Therefore, the γ transition model is chosen for the follow-up study.

Table 3. Comparison of vortex shedding frequency.

Methods	f (Hz)	Δf
Test	1428	
$\gamma-Re_{\theta_t}$ transition model	1361	4.69%
γ transition model	1398	2.10%

4. Suction Control Impact on the Hydrofoil Flow Field

The influence of suction control on the shape of the hydrofoil flow field and the influence rule of some suction parameters are examined in this section using numerical simulation. The characteristics of it before and after suction control are analyzed, including the boundary layer’s characteristics, along with the shape of the vortices in the wake region.

4.1. Structure and Parameters

Referring to aerodynamics [41,42], the selected suction angle has an included angle between the suction direction and the chord direction of 90° , and the diameter of the suction slot is $2.5\%L$. The calculation domain’s spanwise length is $0.3L$. The suction slots are arranged at equal spacing along the spanwise direction of the hydrofoil suction surface, where the slot spacing is $0.15L$. Figure 7 is the structural diagram of the hydrofoil porous distribution suction.

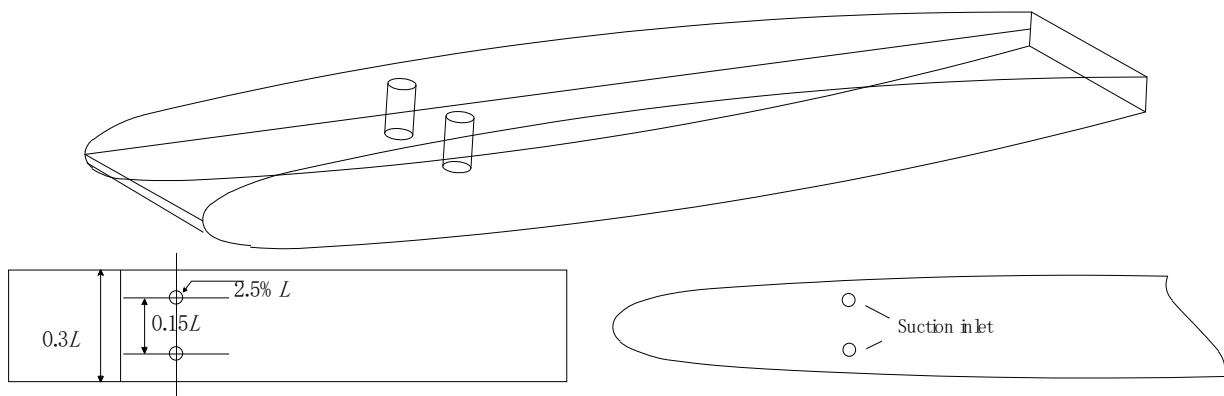


Figure 7. Structural diagram of hydrofoil with suction control.

Regarding suction coefficient C_μ , a dimensionless suction coefficient must first be established in order to assess the suction efficiency, and express the ratio of flow rate to time to measure the influence of suction:

$$C_\mu = \frac{m_s V_s}{0.5 \rho U_\infty} \tag{7}$$

where v represents the speed of the suction slot, m_s is the suction mass flow rate, and A is the area of the hydrofoil. In this study, the transition onset location is $0.85L$, and two suction slot locations are selected: $0.3L$ (leading-edge suction) and $0.7L$ (trailing-edge suction).

The O-grid is selected to be used for the hydrofoil, and the chord length of hydrofoil $L = 0.1$ m is taken as the reference length. The calculation domain of flow direction and perpendicular to flow direction is the same as the baseline hydrofoil (hydrofoil without suction control in Section 3). The number of grid nodes also refers to the number of standard hydrofoil grids. The spanwise calculation domain is $0.3L$, the number of grid nodes is 100, and the spanwise is a periodic boundary condition. To appropriately depict how the suction slot affects the hydrofoil’s flow field structure, the suction slot is refined, wherein the flow direction and the span direction are used to arrange 420 grid nodes, and 240 grid nodes are organized. The computational domain grid structure is depicted in Figure 8.

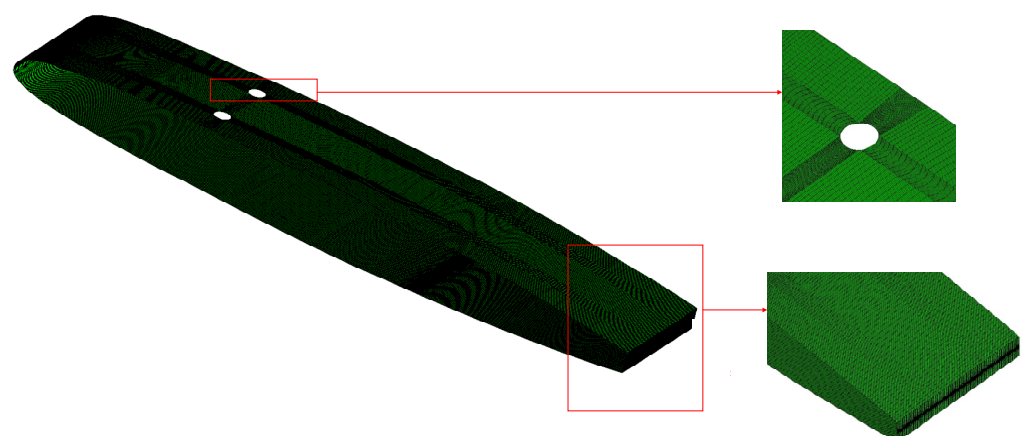


Figure 8. Grid of hydrofoil with suction control.

4.2. Effect of Suction Coefficient

The suction slot design for the suction control effect is heavily influenced by the suction coefficient. Therefore, the suction coefficient is analyzed to explore its influence. The incoming flow velocity is 20 m/s ($Re_L = 2.0 \times 10^6$), and the flow around the hydrofoil with suction control is numerically simulated. To determine how suction control affects the

hydrofoil's flow field structure, the calculation results are compared to those of a normal hydrofoil without suction (Baseline).

Figure 9 depicts the variation in the lift coefficient C_L and drag coefficient C_D with various suction coefficients. As the suction coefficient rises, the lift coefficient shifting trend also rises. Suction control considerably improves the lift coefficient when the suction coefficient is small ($C_\mu < 0.002$). In the range of $C_\mu = 0.002$ – 0.010 , the lift coefficient first increases rapidly and then gradually as the suction coefficient increases. When the suction coefficient is small ($C_\mu < 0.002$), the drag coefficient has a small increase and then begins to decline. After the suction coefficient $C_\mu > 0.002$, the change is floating up and down. The overall trend of the drag coefficient is to decline as the suction coefficient increases, and the range of change is small. The changing trend of the lift/drag ratio is similar to that of the lift coefficient, which gradually increases with the increase in the suction coefficient, but its growth rate is variable. Since the growth rate of the lift coefficient is almost constant, the changing trend of the lift/drag ratio depends on the change in the drag coefficient.

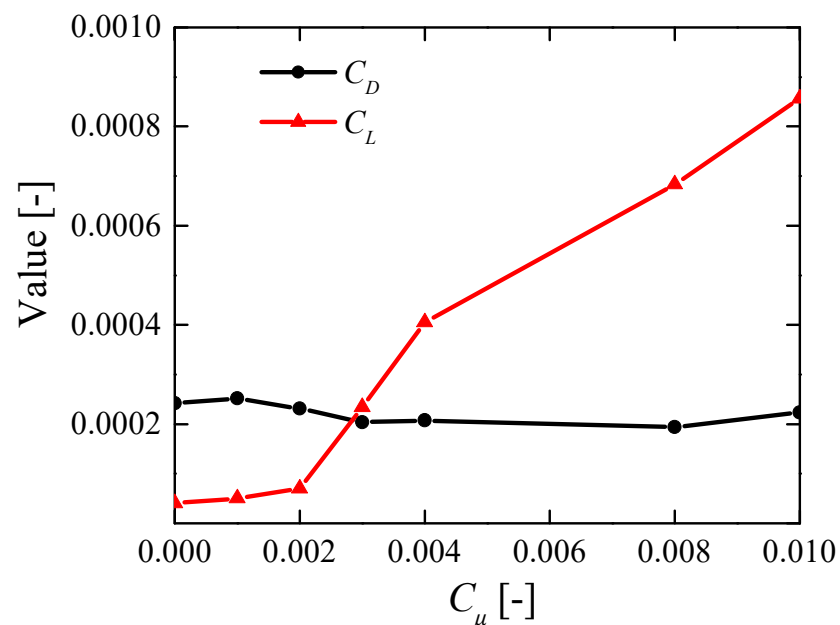


Figure 9. Variation of the lift and drag coefficients with the suction coefficient.

By absorbing the low-energy fluid, the suction can boost the flow momentum and increase resistance to the reverse pressure gradient, to achieve the control effect. Therefore, the changes to the boundary layer need to be examined and discussed. To examine how the suction coefficient affects the hydrofoil surface's transition position, Figure 10 represents the time-averaged friction coefficient C_f of the hydrofoil at various suction speeds. The trend at five suction coefficients is consistent. The friction coefficient increases suddenly near the suction position and decreases slowly with the distance from the suction position. When the suction coefficient is small ($C_\mu < 0.003$), in conjunction with the rising suction coefficient, the friction coefficient rises. However, the subsequent change rule is not uniform. From the curve, when the suction coefficient $C_\mu = 0.003$, the friction coefficient has a downward trend of near $0.85L$, and the transition occurs currently. However, there is no such phenomenon after the suction control is applied, demonstrating that the hydrofoil surface transition can be delayed by the suction control.

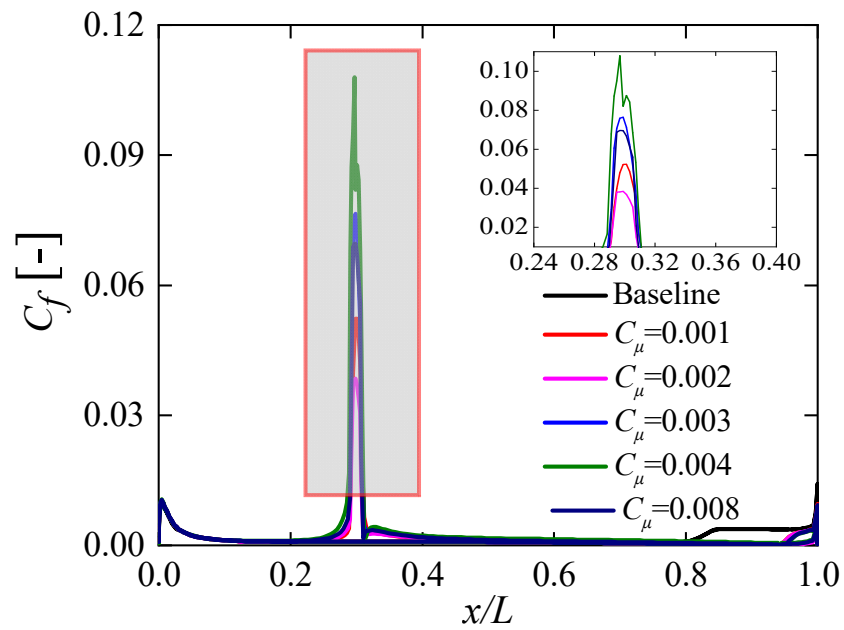


Figure 10. Changes in friction coefficient with changes in suction coefficient.

Figure 11 shows the changes in the wake of a hydrofoil under different suction coefficients. The introduction of suction holes results in significant changes in the strength and range of the wake. As the suction coefficient increases, the strength of the hydrofoil wake decreases significantly.

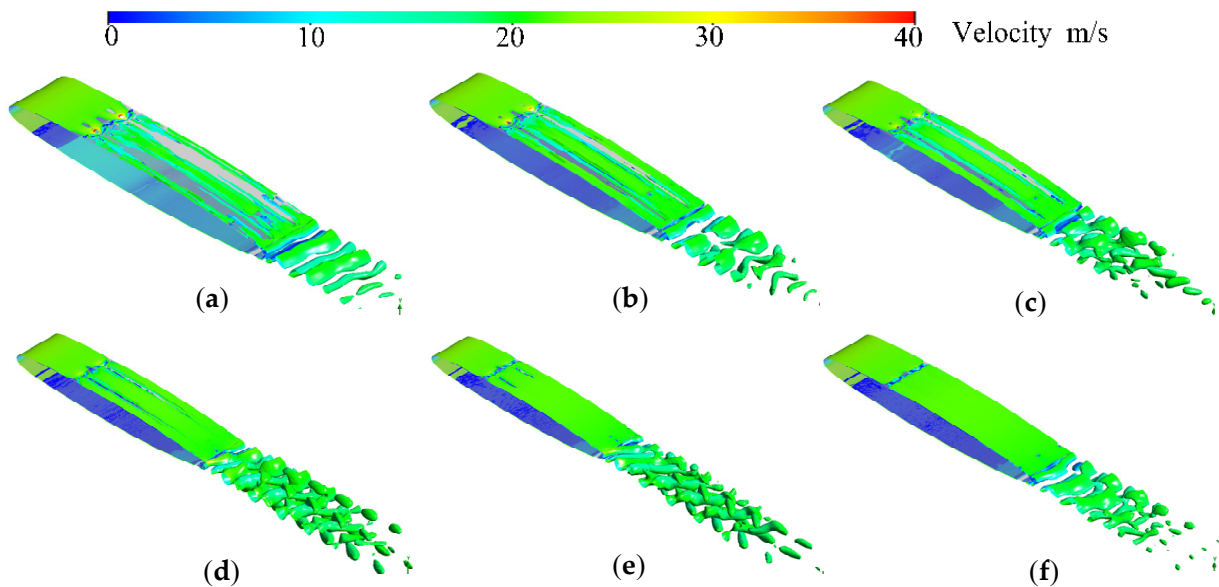


Figure 11. Changes in friction coefficient with changes in suction coefficient. (a) $C_\mu = 0.001$, (b) $C_\mu = 0.003$, (c) $C_\mu = 0.004$, (d) $C_\mu = 0.006$, (e) $C_\mu = 0.008$, (f) $C_\mu = 0.01$.

To quantitatively analyze the effect of suction on vortex shedding in the wake area, Figure 12 shows the frequency of vortex shedding at different suction coefficients. The vortex shedding frequency decreases after the suction control is applied. As the suction coefficient rises, the frequency value does not change regularly, and the frequency decreases ranged from 6% to 10%. When the suction coefficient $C_\mu = 0.001$, the vortex shedding frequency in the wake region reaches the minimum.

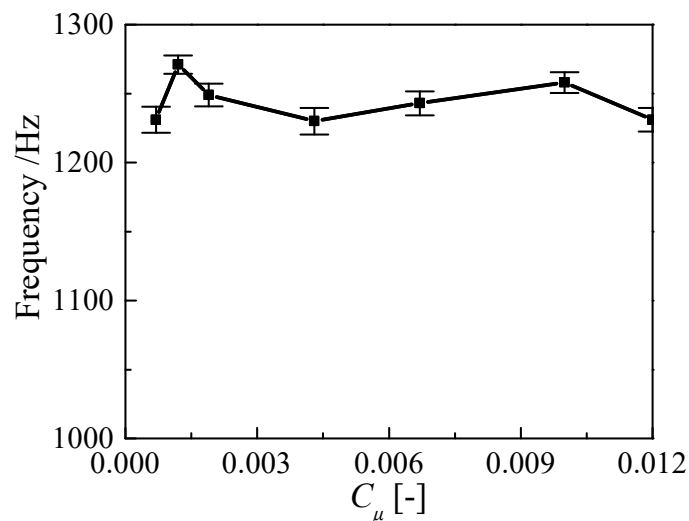


Figure 12. Comparison of vortex shedding frequency and velocity fluctuation with different suction coefficients.

4.3. Effect of Suction Position

The boundary layer low-energy fluid can be absorbed by suction, reduce the momentum loss layer, delay the occurrence of transition, and have an important impact on the vortex in the wake region. However, the specific effect of suction position on suction control needs further study. The inflow conditions in this section are the same as those in Section 4.2. Select the working condition in which the momentum loss in the boundary layer and the velocity fluctuation amplitude in the wake region is the smallest in the previous section, namely, the suction coefficient $C_\mu = 0.003$. Conduct the numerical simulation of the flow around the hydrofoil with suction control and compare the calculation results with the standard hydrofoil without suction to analyze how suction control affects the hydrofoil flow field structure. The suction positions are $0.3L$ (leading-edge suction) and $0.7L$ (trailing-edge suction).

Figure 13 shows the cross-sectional view of the hydrofoil corresponding to the leading-edge suction and the trailing-edge suction. The leading-edge suction slots can reduce the generation of wake by extracting liquid from the leading edge of the hydrofoil, the pressure and the strength of the vortex at the leading edge are reduced, thus the generation of the wake is reduced. The trailing-edge suction hole can affect the magnitude of lift and drag by adjusting the pressure distribution on the hydrofoil surface. Appropriate trailing-edge suction slot control can increase the lift of the hydrofoil and reduce drag.

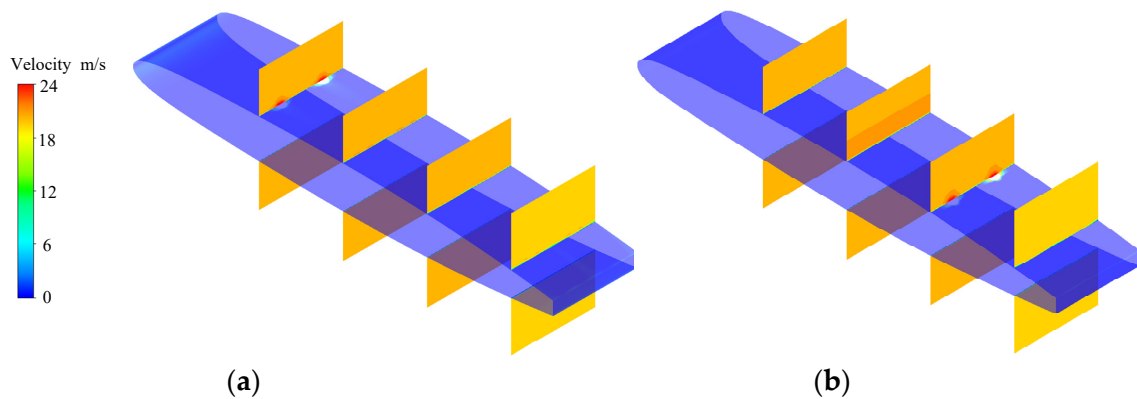


Figure 13. Change of boundary layer momentum and displacement thickness with suction coefficient. (a) leading-edge suction, (b) trailing-edge suction.

Figure 14 presents the boundary layer velocity distribution for various suction positions at the same suction coefficient. Distributions of the boundary layer average velocities over time for $x/L = 0.1, 0.2, 0.4, 0.6, 0.8,$ and 0.9 , where x/L is the ratio of the chord lengths, and 0.99 of the hydrofoils is selected, respectively. The velocity distribution curves for $x/L = 0.2, 0.4, 0.6, 0.8,$ and 0.9 allow for unambiguous observation and analysis of the velocity distribution at various hydrofoil boundary layer sites, and 0.99 positions are shifted by $1.0, 2.0, 3.0, 4.0, 5.0,$ and 6.0 units along the abscissa. When considering the leading-edge suction, as well as the trailing-edge suction, the boundary layer velocity distribution is wider than the hydrofoil typical distribution. From the suction position, the average flow direction velocity gradient increases. The velocity gradient of the leading-edge suction at $x/L = 0.4\sim 0.6$ changes greatly compared with the standard hydrofoil, and the velocity gradient increases rapidly, while the trailing-edge suction does not change at this position. At the position of $x/L = 0.9\sim 0.99$, because of the suction created by the leading and trailing edges, the speed difference between the two surfaces grows, and the velocity profile of the trailing edge suction is plump, but the difference between these two methods is small.

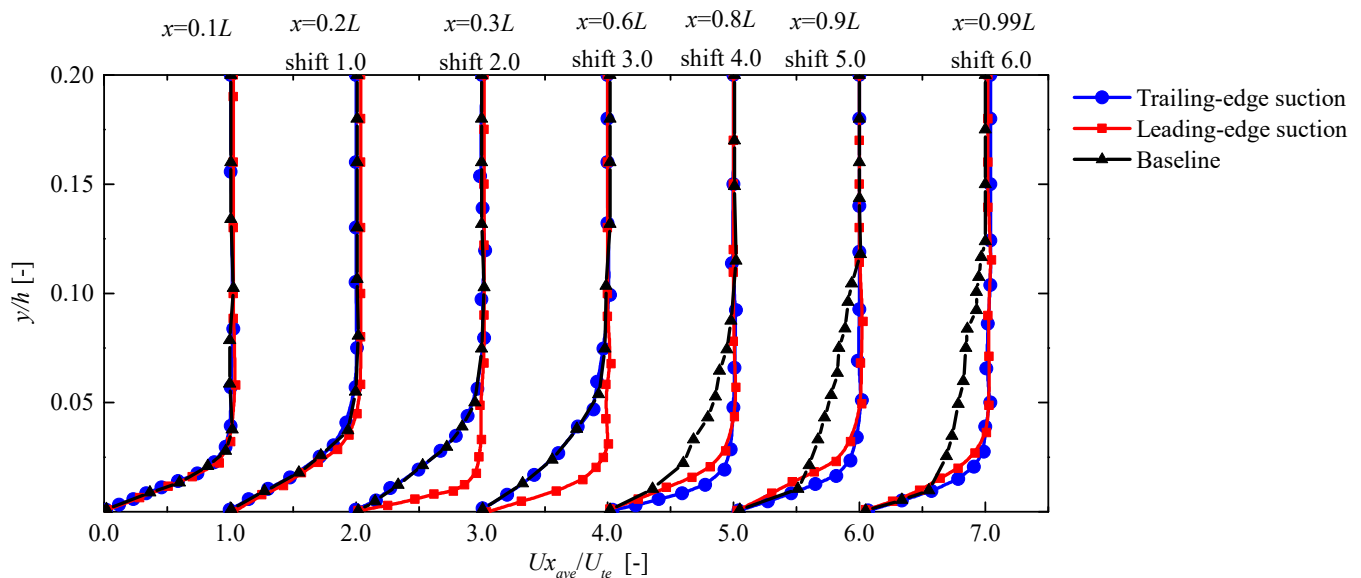


Figure 14. Boundary layer flow direction time-average velocity distribution at various suction positions.

Figure 15 displays the distribution of momentum thickness and displacement thickness under the same suction coefficient at different suction positions. The trailing-edge suction’s total value is greater than the leading-edge suction’s displacement thickness. Considering the displacement thickness definition, the loss of the leading-edge suction mass flow can be reduced more. The distribution of momentum thickness resembles that of displacement thickness, and the leading-edge suction boundary layer experiences less momentum loss than that of the trailing-edge suction.

Figure 16 shows the vorticity of different suction positions. The leading-edge suction control effect is better than the standard hydrofoil. With leading-edge suction, the periodic shedding vortices are somewhat constrained, and the number of vortices in the wake area is lessened. The vorticity diagram of the trailing-edge control has no obvious difference from the standard hydrofoil.

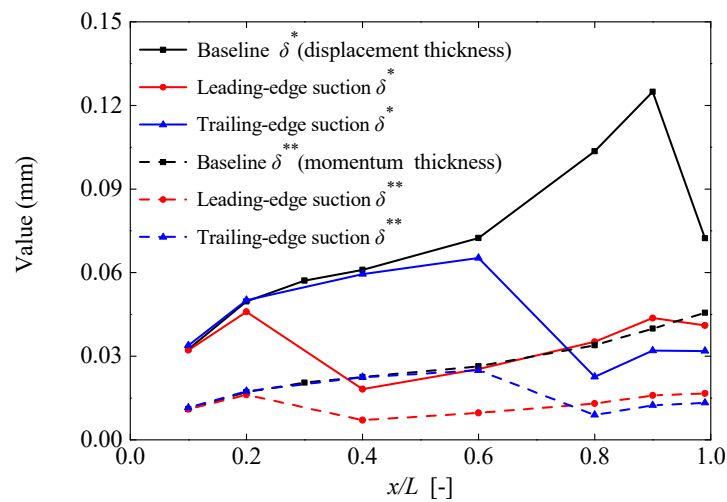


Figure 15. Change of boundary layer momentum and displacement thickness with suction coefficient.

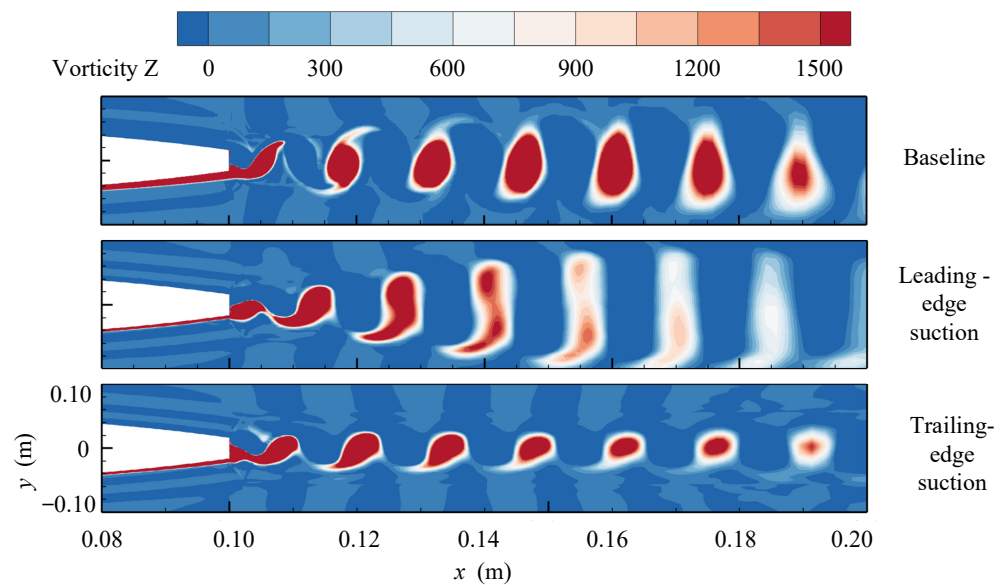


Figure 16. Vorticity diagram of different suction positions.

Figure 17 shows the velocity distribution in the wake area at distinct suction positions. Select the velocity distribution of hydrofoil $x = L + 2h$, $x = L + 3h$, $x = L + 4h$, $x = L + 5h$, and $x = L + 10h$, respectively. Figure 17a is the time-averaged stream-wise velocity, and Figure 17b is the time-averaged transverse velocity to the flow direction. Figure 17c is the stream-wise velocity fluctuations, and Figure 17d is transverse velocity fluctuations. In order to properly see and study the velocity distribution at various locations in the hydrofoil wake, the velocity distribution curves at $x = L + 2h$, $x = L + 3h$, $x = L + 4h$, $x = L + 5h$, and $x = L + 10h$ positions are moved several unit lengths along the abscissa. The wake region averaged velocity peaks in the orientations of x and y rise, and the peak value of velocity fluctuation decreases, regardless of the leading-edge or trailing-edge suction. From Figure 17a,b, the leading-edge suction peak value of the time average velocity in the x and y directions is lower than that of the trailing-edge suction, but at $x = L + h$, the peak value of the y direction velocity of the leading-edge suction is slightly less. From Figure 17c,d, the leading-edge suction peak value of velocity fluctuation is bigger than the trailing-edge suction, and this difference gradually decreases as it is far away from the trailing edge.

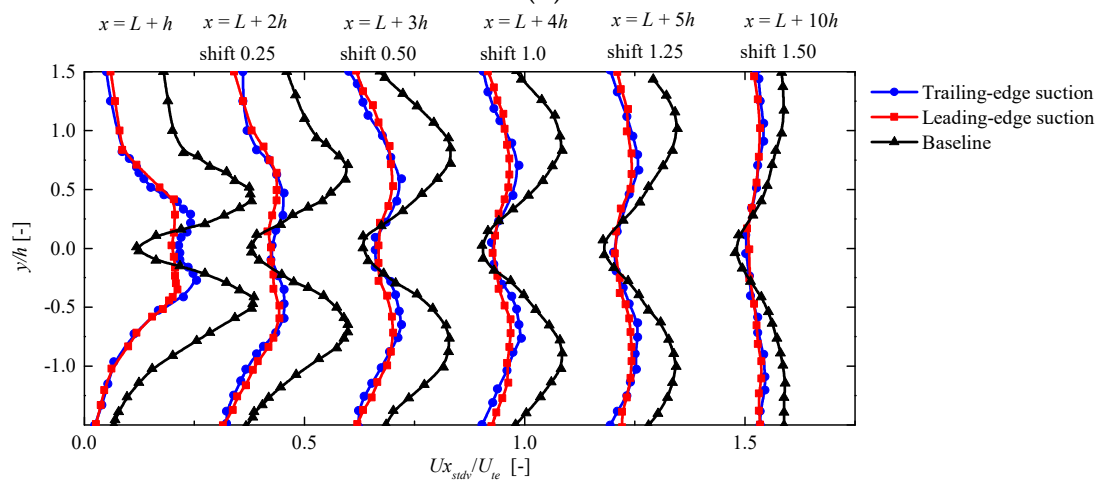
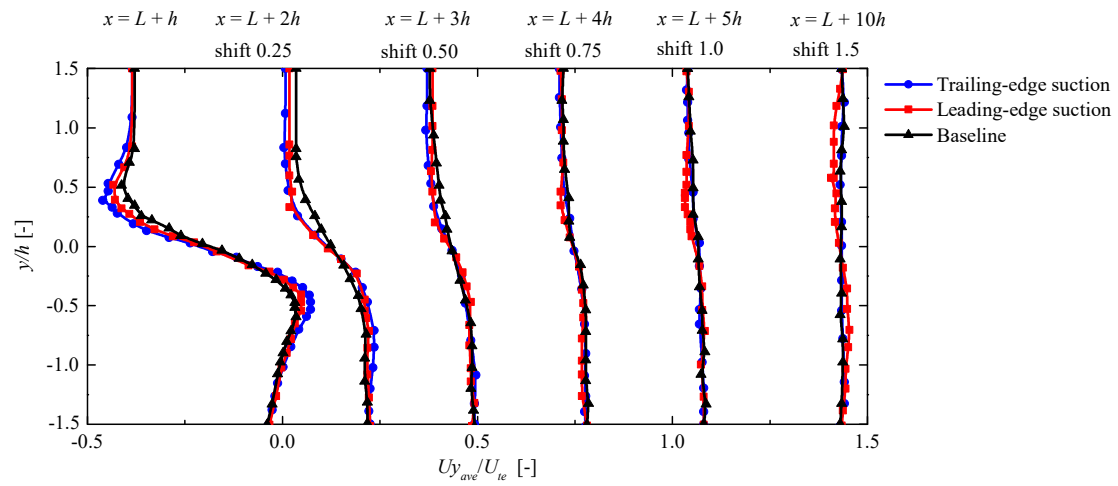
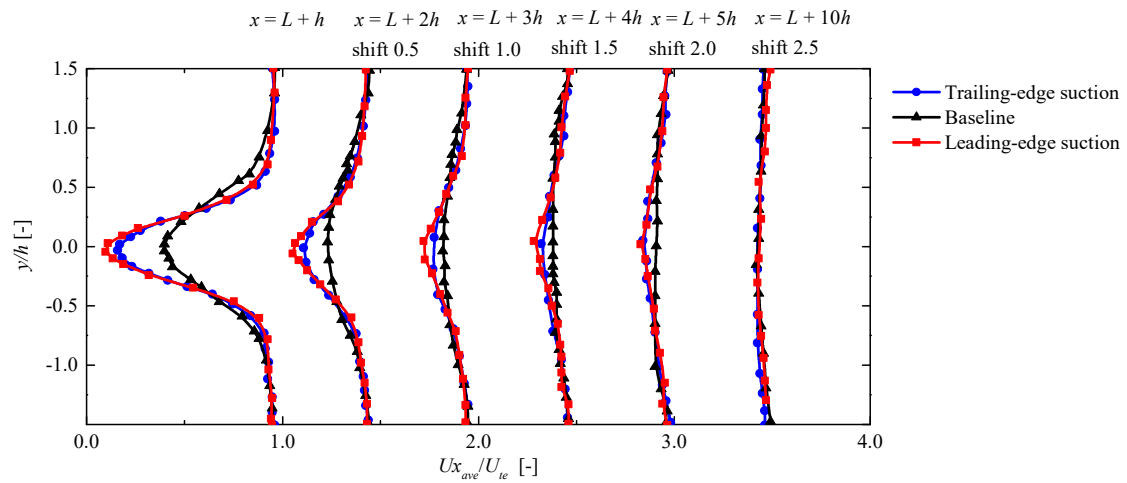


Figure 17. Cont.

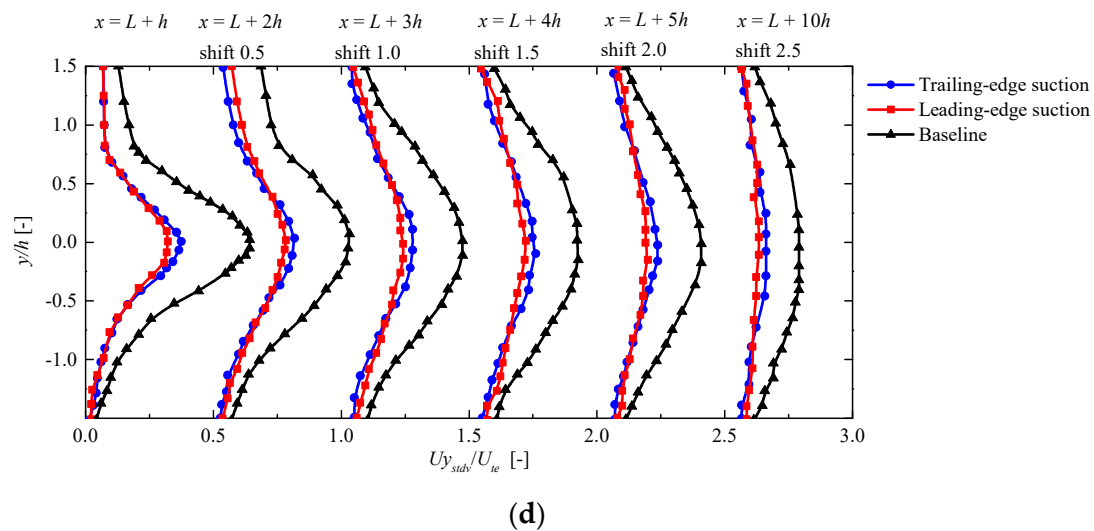


Figure 17. Velocity distribution in wake area at different suction positions. (a) stream-wise velocity profiles; (b) transverse velocity profiles; (c) stream-wise velocity fluctuations; (d) transverse velocity fluctuations.

5. Conclusions

With the NACA0009 blunt trailing edge hydrofoil serving as the focus of the investigation, the impact of suction control on the flow field based on the γ transition model was studied, and the conclusions are obtained as follows.

- (1) The transition model can be applied to effectively forecast the features of the flow field within the boundary layer and the wake area, among which the γ transition model is better than the $\gamma-Re_{\theta t}$ model.
- (2) Adopting suction control, the hydrofoil experiences an increase in its lift/drag ratio when it gets more efficient. The momentum and mass flow loss in the boundary layer decreases, the velocity gradient increases, and the transition position is delayed. The wake zone experiences a drop in terms of the regularity of vortex shedding; moreover, the peak value of velocity fluctuation also experiences a decrease.
- (3) When the suction coefficient $C_{\mu} = 0.003$, the thinnest layers in the boundary layer are those with momentum and displacement, and the velocity fluctuation amplitude in the wake region is the smallest. When the suction slots are placed at the leading edge, the momentum loss in the boundary layer is small, and the velocity fluctuation intensity in the wake region is weak.

This study has examined the impact of both the suction coefficient and suction position on the flow field structure of a hydrofoil, presenting the possibility of exploring alternative suction methods in future investigations. A comprehensive analysis of suction parameters, encompassing multiple factors and accounting for their interdependencies, is recommended for a more in-depth understanding of the subject.

Author Contributions: Software, P.Y.; Validation, H.Y. and C.Z.; Writing—original draft, C.Y.; investigation, Y.R.; Supervision, Y.H. and Y.Z. All authors have read and agreed to the published version of the manuscript.

Funding: National Natural Science Foundation of China (No.52209109, No.52271275), the Open Research Subject of Key Laboratory of Fluid and Power Machinery (Xihua University), the Ministry of Education (grant number LTDL-2022005), and the Scientific Research Start-up Funding, Hohai University (1047/423160). The APC was funded by the Scientific Research Start-up Funding, Hohai University (1047/423160).

Data Availability Statement: Not applicable.

Acknowledgments: The authors appreciated the High-Performance Computing of Hohai University and China Agricultural University.

Conflicts of Interest: The authors declare no conflict of interest.

Nomenclature

L	chord length, m
B	spanwise width, m
h	height of blunt edge, m
γ	intermittent factor
Re_{θ_t}	transition momentum thickness Reynolds number
Re_{θ_c}	transition critical momentum thickness Reynolds number
C_f	friction coefficient
C_μ	suction coefficient
v	velocity of the suction slot, m/s
δ^*	displacement thickness, mm
δ^{**}	momentum thickness, mm
GCI	grid convergence index

References

- Kan, K.; Chen, H.; Zheng, Y.; Zhou, D.; Binama, M.; Dai, J. Transient characteristics during power-off process in a shaft extension tubular pump by using a suitable numerical model. *Renew. Energy* **2021**, *164*, 109–121. [\[CrossRef\]](#)
- Luo, H.; Zhou, P.; Shu, L.; Mou, J.; Zheng, H.; Jiang, C.; Wang, Y. Energy Performance Curves Prediction of Centrifugal Pumps Based on Constrained PSO-SVR Model. *Energies* **2022**, *15*, 3309. [\[CrossRef\]](#)
- Rashidi, S.; Hayatdavoodi, M.; Esfahani, J.A. Vortex shedding suppression and wake control: A review. *Ocean Eng.* **2016**, *126*, 57–80. [\[CrossRef\]](#)
- Sun, J.; Ottavy, X.; Liu, Y.; Lu, L. Corner separation control by optimizing blade end slots in a linear compressor cascade. *Aerosp. Sci. Technol.* **2021**, *114*, 106737. [\[CrossRef\]](#)
- Akhter, M.Z.; Omar, F.K. Review of flow-control devices for wind-turbine performance enhancement. *Energies* **2021**, *14*, 1268. [\[CrossRef\]](#)
- Prandtl, L. Über Flüssigkeitsbewegung bei sehr kleiner Reibung. In Proceedings of the III Internationalen Mathematiker-Kongresses, Heidelberg, Germany, 8–13 August 1904.
- Lei, J.; Liu, Q.; Li, T. Suction control of laminar separation bubble over an airfoil at low Reynolds number. *Proc. Inst. Mech. Eng. Part G J. Aerosp. Eng.* **2019**, *233*, 81–90. [\[CrossRef\]](#)
- Wang, J.; Huang, S.; Hou, L.; Wang, Y. Influence of suction flow control on energy extraction characteristics of flapping foil. *Int. J. Green Energy* **2022**, *19*, 888–903. [\[CrossRef\]](#)
- Fahland, G.; Stroh, A.; Frohnapfel, B.; Atzori, M.; Vinuesa, R.; Schlatter, P.; Gatti, D. Investigation of blowing and suction for turbulent flow control on airfoils. *AIAA J.* **2021**, *59*, 4422–4436. [\[CrossRef\]](#)
- Kornilov, V. Combined Blowing/Suction Flow Control on Low-Speed Airfoils. *Flow Turbul. Combust.* **2021**, *106*, 81–108. [\[CrossRef\]](#)
- Chen, Z.; Shi, Z.; Chen, S.; Yao, Z. Stall flutter suppression of NACA 0012 airfoil based on steady blowing. *J. Fluids Struct.* **2022**, *109*, 103472. [\[CrossRef\]](#)
- Rosas, C.R. *Numerical Simulation of Flow Separation Control by Oscillatory Fluid Injection*; Texas A&M University: College Station, TX, USA, 2005; pp. 124–168.
- Beliganur, N.K.; Raymond, P. Application of evolutionary algorithms to flow control optimization. *Rep. Univ. Kentucky* **2007**.
- Akcayoz, E.; Tuncer, I.H. Numerical investigation of flow control over an airfoil using synthetic jets and its optimization. In Proceedings of the 5th Ankara International Aerospace Conference, Ankara, Turkey, 17–19 August 2009.
- Muddada, S.; Patnaik, B. Active flow control of vortex induced vibrations of a circular cylinder subjected to non-harmonic forcing. *Ocean Eng.* **2017**, *142*, 62–77. [\[CrossRef\]](#)
- Ramsay, J.; Sellier, M.; Ho, W.H. Non-uniform suction control of flow around a circular cylinder. *Int. J. Heat Fluid Flow* **2020**, *82*, 108559. [\[CrossRef\]](#)
- Akbarzadeh, P.; Akbarzadeh, E. Hydrodynamic characteristics of blowing and suction on sheet-cavitating flows around hydrofoils. *Ocean Eng.* **2016**, *114*, 25–36. [\[CrossRef\]](#)
- De Giorgi, M.G.; Fontanarosa, D.; Ficarella, A. Active Control of Unsteady Cavitating Flows Over Hydrofoil. *J. Fluids Eng.* **2020**, *142*, 111201. [\[CrossRef\]](#)
- Royset, J.O.; Bonfiglio, L.; Vernengo, G.; Brizzolara, S. Risk-Adaptive Set-Based Design and Applications to Shaping a Hydrofoil. *J. Mech. Des.* **2017**, *139*, 101403. [\[CrossRef\]](#)
- Wang, H.; Ding, L.; Zhang, L.; Zou, Q.; Sharma, R.N. Control of two-degree-of-freedom vortex induced vibrations of a circular cylinder using synthetic Jets: Effect of synthetic jet orientation angle and phase difference. *Ocean Eng.* **2020**, *217*, 107906. [\[CrossRef\]](#)

21. Goodarzi, M.; Rahimi, M.; Fereidouni, R. Investigation of active flow control over NACA0015 airfoil via blowing. *Int. J. Aerosp. Sci.* **2012**, *1*, 57–63.
22. Chen, Q.; Liu, Y.; Wu, Q.; Wang, Y.; Liu, T.; Wang, G. Global cavitation patterns and corresponding hydrodynamics of the hydrofoil with leading edge roughness. *Acta Mech. Sin.* **2020**, *36*, 1202–1214. [[CrossRef](#)]
23. Yousefi, K.; Saleh, R.; Zahedi, P. Numerical study of blowing and suction slot geometry optimization on NACA 0012 airfoil. *J. Mech. Sci. Technol.* **2014**, *28*, 1297–1310. [[CrossRef](#)]
24. Fransson, J.; Konieczny, P.; Alfredsson, P. Flow around a porous cylinder subject to continuous suction or blowing. *J. Fluids Struct.* **2004**, *19*, 1031–1048. [[CrossRef](#)]
25. Moffat, R.J.; Kays, W.M. The turbulent boundary layer on a porous plate: Experimental heat transfer with uniform blowing and suction. *Int. J. Heat Mass Transf.* **1968**, *11*, 1547–1566. [[CrossRef](#)]
26. Durbin, P.A. Some Recent Developments in Turbulence Closure Modeling. *Annu. Rev. Fluid Mech.* **2018**, *50*, 77–103. [[CrossRef](#)]
27. Menter, F.R.; Langtry, R.B.; Likki, S.R.; Suzen, Y.B.; Huang, P.G.; Völker, S. A Correlation-Based Transition Model Using Local Variables—Part I: Model Formulation. *J. Turbomach.* **2006**, *128*, 413–422. [[CrossRef](#)]
28. Menter, F.R.; Matyushenko, A.; Lechner, R.; Stabnikov, A.; Garbaruk, A. An Algebraic LCTM Model for Laminar–Turbulent Transition Prediction. *Flow Turbul. Combust.* **2022**, *109*, 841–869. [[CrossRef](#)]
29. Rahman, M.M.; Hasan, K.; Pan, H. Capturing transition around low-Reynolds number hydrofoil with zero-equation transition model. *Phys. Fluids* **2022**, *34*, 074115. [[CrossRef](#)]
30. Zeng, Y.; Yao, Z.; Gao, J.; Hong, Y.; Wang, F.; Zhang, F. Numerical Investigation of Added Mass and Hydrodynamic Damping on a Blunt Trailing Edge Hydrofoil. *J. Fluids Eng.* **2019**, *141*, 081108. [[CrossRef](#)]
31. Zeng, Y.; Zhang, M.; Du, Y.; Yao, Z.; Wu, Q.; Wang, F. Influence of attack angle on the hydrodynamic damping characteristic of a hydrofoil. *Ocean Eng.* **2021**, *238*, 109692. [[CrossRef](#)]
32. Ye, C.L.; Wang, C.Y.; Zi, D.; Tang, Y.; van Esch, B.P.; Wang, F.J. Improvement of the SST γ -Re θ t transition model for flows along a curved hydrofoil. *J. Hydrodyn.* **2021**, *33*, 520–533. [[CrossRef](#)]
33. Ye, C.; Tang, Y.; An, D.; Wang, F.; Zheng, Y.; van Esch, B. Investigation on stall characteristics of marine centrifugal pump considering transition effect. *Ocean Eng.* **2023**, *280*, 114823. [[CrossRef](#)]
34. Menter, F.R.; Smirnov, P.E.; Liu, T.; Avancha, R. A One-Equation Local Correlation-Based Transition Model. *Flow Turbul. Combust.* **2015**, *95*, 583–619. [[CrossRef](#)]
35. Wang, R.; Xiao, Z. Transition effects on flow characteristics around a static two-dimensional airfoil. *Phys. Fluids* **2020**, *32*, 035113. [[CrossRef](#)]
36. Cui, B.; Wang, X.; Wang, R.; Xiao, Z. Numerical investigation of transonic axial compressor rotor flows using an improved transition-sensitized turbulence model. *Phys. Fluids* **2021**, *33*, 035149. [[CrossRef](#)]
37. Rubino, G.; Visonneau, M. Improved crossflow transition predictions for the one-equation γ transition model. *Comput. Fluids* **2022**, *245*, 105580. [[CrossRef](#)]
38. Ausoni, P. *Turbulent Vortex Shedding from a Blunt Trailing Edge Hydrofoil*; EPFL: Lausanne, Switzerland, 2009; pp. 56–168. [[CrossRef](#)]
39. Wang, C.; Wang, F.; Li, C.; Chen, W.; Wang, H.; Lu, L. Investigation on energy conversion instability of pump mode in hydro-pneumatic energy storage system. *J. Energy Storage* **2022**, *53*, 105079. [[CrossRef](#)]
40. Roache, P.J. *Verification and Validation in Computational Science and Engineering*; Hermosa Publishers: Albuquerque, NM, USA, 1998.
41. Li, D.; Yang, Q.; Yang, W.; Chang, H.; Wang, H. Bionic leading-edge protuberances and hydrofoil cavitation. *Phys. Fluids* **2021**, *33*, 093317. [[CrossRef](#)]
42. Moussavi, S.A.; Ghaznavi, A. Effect of boundary layer suction on performance of a 2 MW wind turbine. *Energy* **2021**, *232*, 121072. [[CrossRef](#)]

Disclaimer/Publisher’s Note: The statements, opinions and data contained in all publications are solely those of the individual author(s) and contributor(s) and not of MDPI and/or the editor(s). MDPI and/or the editor(s) disclaim responsibility for any injury to people or property resulting from any ideas, methods, instructions or products referred to in the content.